applied optics

Development of an immersive virtual reality head-mounted display with high performance

Yunqi Wang,[1,2,*] Weiqi Liu,[1,2] Xiangxiang Meng,[3] Hanyi Fu,[2] Daliang Zhang,[2] Yusi Kang,[2] Rui Feng,[2] Zhonglun Wei,[2] Xiuqing Zhu,[4] and Guohua Jiang[4]

[1]University of Chinese Academy of Science, Beijing 100049, China
[2]First Department of Space Optics, Changchun Institute of Optics, Fine Mechanics and Physics, Chinese Academy of Science, Changchun, Jilin 130033, China
[3]Shangdong Institute of Aerospace Electronics Technology, Yantai, Shandong 264003, China
[4]Key Laboratory of Human Factors Engineering, China Astronaut Training Center, Beijing 100094, China
*Corresponding author: doctorwho_wangyq@163.com

Received 25 April 2016; revised 16 June 2016; accepted 5 July 2016; posted 27 July 2016 (Doc. ID 263921); published 26 August 2016

To resolve the contradiction between large field of view and high resolution in immersive virtual reality (VR) head-mounted displays (HMDs), an HMD monocular optical system with a large field of view and high resolution was designed. The system was fabricated by adopting aspheric technology with CNC grinding and a high-resolution LCD as the image source. With this monocular optical system, an HMD binocular optical system with a wide-range continuously adjustable interpupillary distance was achieved in the form of partially overlapping fields of view (FOV) combined with a screw adjustment mechanism. A fast image processor-centered LCD driver circuit and an image preprocessing system were also built to address binocular vision inconsistency in the partially overlapping FOV binocular optical system. The distortions of the HMD optical system with a large field of view were measured. Meanwhile, the optical distortions in the display and the trapezoidal distortions introduced during image processing were corrected by a calibration model for reverse rotations and translations. A high-performance not-fully-transparent VR HMD device with high resolution (1920 × 1080) and large FOV [141.6°(H) × 73.08°(V)] was developed. The full field-of-view average value of angular resolution is 18.6 pixels/degree. With the device, high-quality VR simulations can be completed under various scenarios, and the device can be utilized for simulated trainings in aeronautics, astronautics, and other fields with corresponding platforms. The developed device has positive practical significance.

OCIS codes: (080.2740) Geometric optical design; (120.2040) Displays; (120.2820) Heads-up displays; (120.3620) Lens system design; (120.4570) Optical design of instruments; (220.0220) Optical design and fabrication.

http://dx.doi.org/10.1364/AO.55.006969

1. INTRODUCTION

Virtual reality (VR) technology, also known as virtual simulation or virtual analog technology, is often utilized to simulate real environments with a virtual environment generated by a particular system. The technology comprehensively utilizes a computer graphics system and various control interface devices to allow people to experience a strong sense of immersion in the interactive 3D digital environment generated on a computer with audio, visual, and tactile effects [1]. Since its introduction in 1968, the technology has been eliciting much attention. The proportion of educational and entertainment applications exceeded 20%, and the proportion of military and aerospace applications exceeded 13% [2–4]. A head-mounted display (HMD), as the main carrier of VR technology, receives computer-simulated virtual scene images and inputs them into user brains through human eyes. An HMD can be used not only as the virtual scene output module of large-VR devices but also as a portable VR device. Immersion is the main keyword in the definition of VR technology and is the most important measure of VR technology as well [5]. When users wear the high-performance HMD system, a strong sense of immersion can be generated in the user's brain by watching the image output from the HMD system. The high-performance HMD system is mainly the technical support of virtual display technology. Research and development of a high-performance HMD play an important role in promoting the development of VR technology.

HMDs can be classified as augmented reality and immersive [6]. For augmented reality HMDs, users can view scenes in the external world through these HMDs. These displays aim to

provide abundant information to users and generally utilize a fully transparent monocular or binocular optical system. They provide a sense of immersion through external real scenes, and their design mainly features high brightness, high contrast, high resolution, highly informative display content, light weight, and a compact system structure, most of which adopt modern optical technologies such as binary, guided wave, and holographic optics [7–13]. For immersive HMDs, users cannot view external scenes through these displays. The purpose of such displays is to enable high-fidelity simulations of various complex, difficult, and impossible-to-restore scenes so that users can obtain life-like visual immersive experiences in a virtual digital environment simulated by an HMD and complete high-fidelity task trainings. Immersive HMDs create a sense of immersion by relying entirely on their own performance. Large field of view, high resolution, and excellent image quality are the main development trends of immersive VR HMDs [12,14–21].

Currently, single-lens technology is used by Oculus Rift and other commercial VR devices on the market. The image quality in the center field of view is very high, but the image quality of the edge fields of view decline very seriously. The image quality of the whole fields of view cannot be guaranteed. In order to ensure the imaging quality of the full field of view of the VR HMD, a not-fully-transparent VR HMD was investigated in this study to meet the needs of users and improve the performance of immersive VR HMD systems. Aspheric surface technology with large deviation and CNC grinding were applied to design and fabricate an HMD visual optical system that combines the advantages of large field of view, high resolution, and high image quality and could offer a good sense of immersion in the simulated virtual environment. A wide-range, continuous-adjustability interpupillary distance (IPD) was achieved with the lead screw-guide rod adjustment mechanism, thereby improving the wearing comfort level and universality of HMDs. A test platform was built to measure the distortions in the optical system. A translation calibration model was proposed, and an LCD driver and image preprocessing system were built to address binocular vision inconsistency in the partially overlapping fields of view (FOV) binocular optical system and to correct distortions in the system. A high-resolution, intensely immersive, not-fully-transparent VR HMD device with a large FOV was developed. The device can be utilized for education, medicine, aerospace, astronaut training, and other fields and thus has positive practical significance and a reference value.

2. DEVELOPMENT OF AN HMD OPTOMECHANICAL STRUCTURE

A. Immersive HMD

An immersive HMD is a VR display device that uses an optical system to directly present virtual scenes received by the display and generated by the host computer to the human eyes; it works with the human brain to produce a strong sense of immersion. The device consists of four parts: an HMD optical system, a head support structure, an image processing and display unit, and a sensor positioning unit. HMDs can be used alone or as a part of a large-VR simulation equipment together with a central processor and external devices. The constitution and structure of the VR system are shown in Fig. 1.

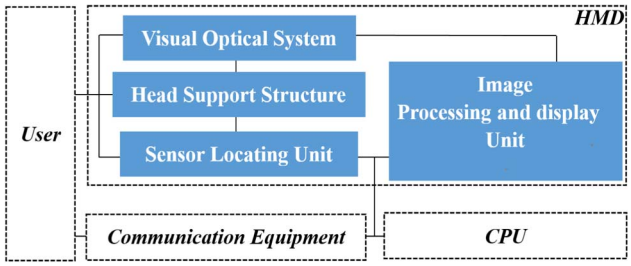

Fig. 1. Constitution and structure of the VR system.

In the HMD system, the head support structure is the "skeleton" of the entire device. It is responsible for fixing the relative position of various subsystems and fixing the device to the user's head. The sensor positioning unit is the "nerve" between the device and the user; it is responsible for information transmission, including digital information transmission between various units and interactive information transmission between the user and the device. The visual optical system, together with the image processing and display unit, constitutes the output end of the device. Users observe the virtual image information processed by the image processing unit and displayed by the display unit through the visual optical system to obtain a sense of immersion in their minds; this is the purpose of the VR simulation. The sensor positioning unit is responsible for gathering information, such as changes in the posture of the user. When an HMD is utilized alone, the sensor positioning and image processing and display units constitute the microprocessor of the HMD. When an HMD is utilized in conjunction with other devices, the microprocessor is connected directly to the central processor to form complex VR simulation equipment for the completion of large-scale VR simulations.

B. Optomechanical Structure of an HMD

Resolution and field of view are the two primary technical indicators of an HMD optical system. The focal length of the system is given by

$$f = \frac{h}{\tan\theta}, \tag{1}$$

where the field angle of the system is denoted by θ, and the resolution of the system is denoted by object height h. When f is a constant, the field angle will decrease with the increase in resolution. How to increase the FOV of an HMD while maintaining high resolution is a significant challenge in this field.

With the rapid development of display unit manufacturing technology, the number and density of display pixels have been constantly increasing, pixel size has been constantly decreasing, and resolution has been constantly improving. These conditions have contributed to the angular resolution in pixels per degree of the HMD and offer numerous image source options for high-performance VR HMDs. To match the high-resolution image source, strict requirements are imposed on the performance of HMD optical systems. After comprehensively considering several factors, such as resolution, contrast, sharpness, power, mechanical dimensions, and weight, a 4.7 in.

Table 1. Initial Structure Parameter

Surface	Radius (mm)	Thickness (mm)	Glass (Index Nd; Abbe Vd)
1(STO)	infinity	22.700	
2	−81.600	7.000	(1.57; 62.9)
3	−24.380	0.300	
4	71.640	9.000	(1.57; 62.9)
5	−69.660	0.200	
6	32.660	14.900	(1.57; 62.9)
7	−34.910	1.600	(1.81; 25.4)
8	31.620	7.400	(1.52; 64.1)
9	infinity	4.330	

Sharp LS047T1SC01K LCD with a 1920 × 1080 resolution was selected as the image source in this study.

The monocular optical system was designed after selecting the source image and resolution. To increase FOV while ensuring resolution, a type I wide-angle eyepiece with a wide FOV and large exit pupil distance was selected as the initial structure. The parameter of the initial structure is given in Table 1, and the structure is shown in Fig. 2.

In such a structure, field curvature was compensated by astigmatism. The pupil diameter of the initial system is 4 mm, while the pupil diameter of human eye is less than 3.04 mm. The luminous intensity value of the LCD is 200–500 cd/m^2. The EPD diameter is set to 3–4 mm for most visual systems such as microscope oculars and telescope eyepieces. However, human eyes can only see objects within 20 deg near the line of sight in the open condition. Human eyes need to look at objects in a wild range by using its rotation. Thus, the EPD of the HMD optical system should be bigger than the other visual system. Generally speaking, considering the weight of the system, the size of the field of view, the immersive virtual reality HMD, and the flight simulation training, the exit pupil diameter of the HMD optical system should be at least more than 7 mm and no more than 10 mm. Thus, the exit pupil diameter was small, and the system was rather cumbersome.

The initial structure was optimized according to its characteristics and design requirements. First, focal length was scaled down to the design value. Second, FOV was gradually enlarged, and the structure parameters were finely adjusted manually to converge light rays. The ZEMAX optimization function with defocused spots was established as an evaluation criterion to

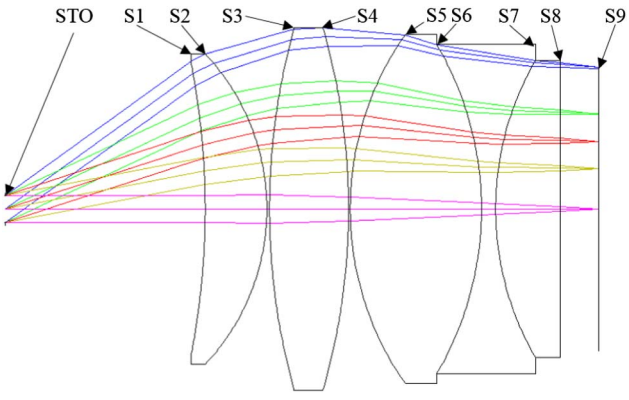

Fig. 2. Optical path diagram of the initial structure.

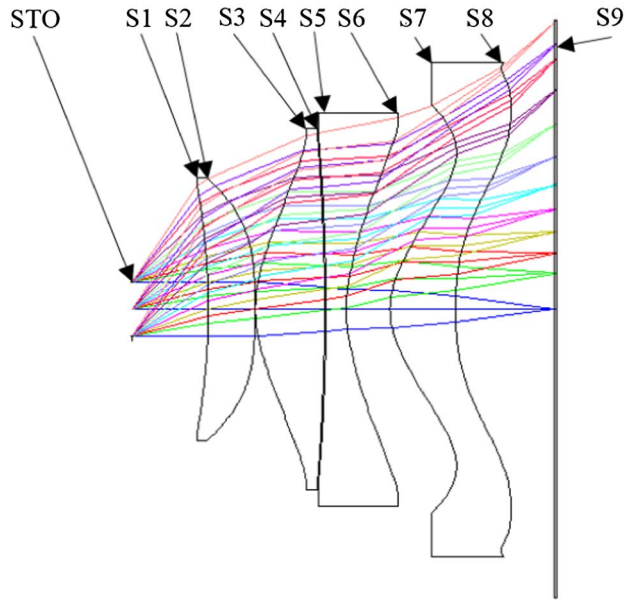

Fig. 3. Monocular optical structure.

perform automatic optimization, with mirror spacing and the radius of the curvature as the optimization variables. During the optimization, three conjoint structures were gradually separated, and the unnecessary optical surface was removed. The entrance pupil diameter was increased, and the exit pupil distance was reduced to meet the design values.

Aspheric optical elements based on the following characteristics were introduced:

$$z = \frac{cr^2}{1 + \sqrt{1 - (K+1)c^2r^2}} + \alpha_1 r^2 + \alpha_2 r^2 + \alpha_3 r^2 + \alpha_4 r^2 + \ldots, \quad (2)$$

where coefficients α_1, α_2, α_3, and α_4 in the equation were included as optimization variables to improve the degree of freedom of the design and the aberration balance of the system. After improving imaging quality through repeated optimization, an HMD monocular optical system was obtained, as shown in Fig. 3. The MTF curve of the system is shown in Fig. 4. The field curvature and distortion of the system are shown in Fig. 5.

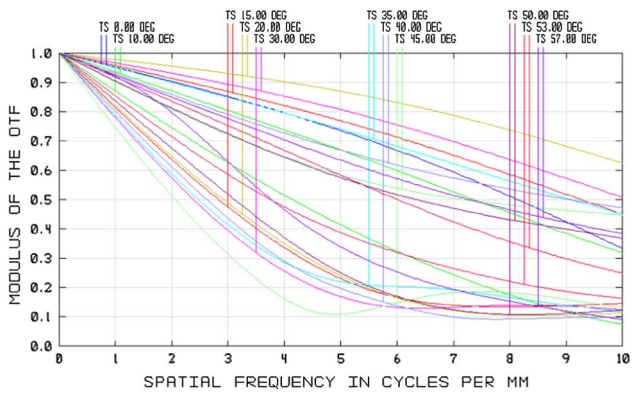

Fig. 4. Diagram of the MTF curve.

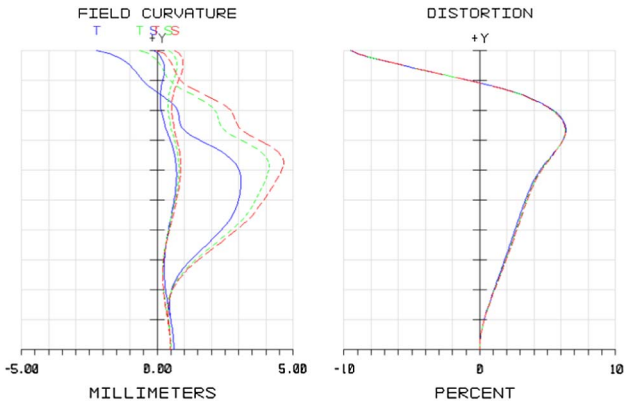

Fig. 5. Diagram of field curvature and distortion.

In terms of material selection and processing, in order to eliminate the aberration of the system and control the distortion of the edge field of view, element 1, element 2, and element 3 were selected for low-density optical glass with a low dispersion coefficient and high refractive index. Meanwhile, element 4 was selected as an eco-friendly, lightweight optical plastic to achieve tolerance, weight loss, and other requirements. Details of the selection of optical elements are shown in Table 2.

Glass aspheric optical elements with large deviations were processed through rough grinding, rounding, CNC grinding, profiler initial inspection, magnetic fluid polishing, and reinspection. Plastic lenses were processed with open molding and turning techniques. Figure 6 shows the actual picture of the finished lens.

Aluminum alloy was selected as the material for the mechanical structure, and processing of the optical tube was completed by integrated processing combined with stress relief heat treatment technologies. To further decrease the weight of the user's head, we removed the excess part of the optical lens. We also separated electronic control devices and helmets. Ultimately, the total weight of the system is less than 1000 g.

Table 2. Details of the Selection of Optical Elements

No.	CDGM (NHG)	SCHOTT	Index N_d	Abbe V_d
Element 1	H-LaF50B	N-LaF35	1.77	49.6
Element 2	H-LaF50B	N-LaF35	1.77	49.6
Element 3	H-ZF52	SFL57	1.85	23.8
Element 4	E48R (optical plastic)		1.53	56

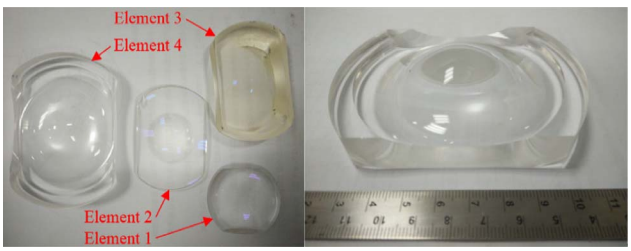

Fig. 6. Image of element 4.

Fig. 7. Image of the HMD monocular optical system.

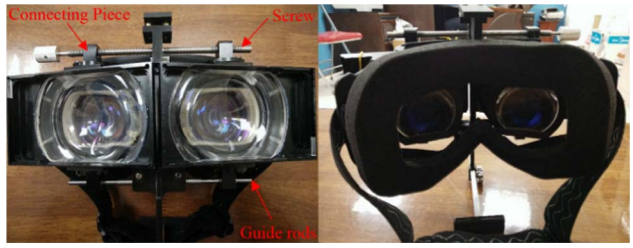

Fig. 8. Assembled HMD binocular optical system.

In the course of the study, we found that the weight of the HMD is a little bit different from the user's head force from the weight of the HMD. Therefore, we can suspend the HMD to reduce the weight of the user's head by using some external suspension equipment in some cases. In addition to this, we believe that the weight of the HMD equipment can be further reduced if the plastic is used to process the barrel and other parts.

Figure 7 shows an actual photograph of the assembled HMD monocular optical system. Based on this monocular optical system, a binocular optical system was implemented with divergent overlapping FOV architecture. First, two monocular lenses were assembled. Second, the two optical tubes were connected with a lead screw at the upper part and a guide rod parallel to it at the lower part by a connecting member into the binocular eyepiece optical tube. Third, the optical axis deflection angles of the two optical tubes were precisely adjusted to allowable tolerance ranges with an angle gauge. Finally, the connector of the two tubes was fixed with a screw to complete the helmet assembly. Figure 8 shows an actual photo of the assembled HMD binocular optomechanical structure. When the lead screw at the upper part is rotated clockwise (counterclockwise), the left and right optical tubes move simultaneously in the same (or opposite) direction to achieve binocular IPD adjustment.

For a VR HMD, the more important parameter is the resolution perceived by the user. It can be angular resolution in pixels per degree, as given in Table 3. It can be seen that the imaging quality of the system in the whole field of view can be ensured.

3. MEASUREMENT OF RELATIVE DISTORTIONS OF THE OPTICAL SYSTEM

Given that the large-FOV HMD optical system has limited ability to balance distortions, further distortion elimination

Table 3. Angular Resolution Value in Pixels/Degree of Each Field of View

FOV(θ) (deg)	F tan(θ) (mm)	Total Pixels	Pixel Increment	Pixels/ Degree
10	6.9	138	138	13.8
20	14.2	284	146	14.6
30	22.5	450	166	16.6
40	32.7	654	204	20.4
50	46.5	930	276	27.6
Average value				18.6

by image processing was performed. The actual amount of distortion in the system would somewhat differ from the design distortion value because of the presence of errors in the processing and adjustment processes. Adequate elimination of residual distortions would be impossible if image processing was performed simply using the design distortion value. Therefore, the distortions in the assembled optical system must be accurately measured. Distortion measurement is an important aspect of helmet displays; it has special significance for subsequent image processing.

A. Distortion Measurement Principle

In optical design, the difference δD between the ideal image height h' and the real image height h is often utilized to represent distortion and is given by

$$\delta D = h - h' = h - f_0 \cdot \tan \omega, \tag{3}$$

where f_0 is the focal length of the central field. Relative distortion is often represented by the percentage q of image height difference δD with respect to the ideal image height as follows:

$$q = \frac{(h - f_0 \cdot \tan \omega)}{f_0 \cdot \tan \omega} \times 100\%. \tag{4}$$

The actual relative distortion of the system can be obtained by measuring and calculating the real image height, ideal image height, and field angle. In this study, a CCD was utilized to capture the image formed on the optical system by a uniform grid plate that has the same size as the LCD. The real image height was obtained by image measurement and conversion. Precise control of the field angle was achieved with a precision turntable, and ideal image height was obtained by calculation. Afterward, relative distortion was calculated with Eq. (3) to complete the measurement.

B. Distortion Measurement Platform

The HMD optical system proposed herein is a large-FOV, medium-accuracy, visual optical system. A measurement platform was built (shown in Fig. 9, topview) based on the measurement principle described in Section 3.A.

First, the system under test was fixed on a precision turntable so that it could rotate synchronously for accurate control of field angle ω. Second, a monochrome grid plate image input generated by the computer program VC++ 6.0 was placed on a high-brightness LED screen on the object plane of the optical system. After slight adjustment, a clear and bright grid plate image was obtained visually. Last, the CCD was placed at the exit pupil of the system so that the various parts of the devices

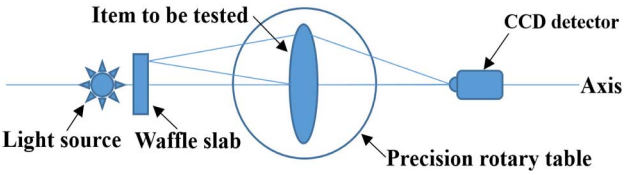

Fig. 9. Schematic of the distortion measurement platform.

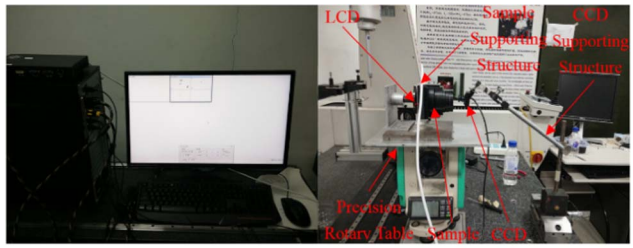

(a) (b)

Fig. 10. Actual photo of the HMD distortion measurement platform. (a) Controlling system. (b) Distortion measurement platform.

were collinear. During measurement, the positions of the LED screen and CCD were kept stationary, and the grid plate image formed on the optical system under test was captured with the CCD. Real image height h was obtained after measurement and conversion of the captured image. By rotating the turntable and accurately recording field angle ω rotated by the turntable, measurement of the real image height in each FOV of the optical system was completed. Figure 10 shows an actual photo of the HMD distortion measurement system. Figure 10(a) shows the distortion measurement controlling system that integrates the HMD image input, CCD image acquisition, and distortion calculation functions. Figure 10(b) presents the measurement platform.

The means of field angle, ideal image height (height of image, which is at the focal plane of the optical system), and real image height obtained through multiple measurements of relevant data in this section are shown in Table 4. It should be noted that a grid unit was each small grid on the checkboard pattern, where the edge length of each grid unit was set to 1 cm. In the process of the data recording, we used "grid unit" as our unit of measurement to measure real image height and ideal image height.

The data in Table 1 were substituted into the relative distortion calculation formula, Eq. (4), to obtain the relative distortions in each FOV of the optical system. The results are shown in Table 5.

4. DEVELOPMENT OF THE LCD DRIVER AND PREPROCESSING SYSTEM

The LCD driver and preprocessing system consisted of two parts. The first part, the driver circuit, is mainly responsible for lighting the LCD so that the LCD could display images normally. The second part, the preprocessing circuit, is mainly responsible for preprocessing images, correcting distortions, and eliminating binocular vision inconsistencies. The image

Table 4. Parameters of View Field, Real Image Height, and Ideal Image Height

No.	View Field (ω)	Real Image Height(b)/ grid unit	Ideal Image Height($f_0 \tan \omega$)/ grid unit
0	0°0′0″	0	0
1	7°12′0″	1	1
2	13°28′0″	2	1.895549
3	19°33′0″	3	2.810914
4	25°31′30″	4	3.779891
5	31°16′0″	5	4.806586
6	36°51′0″	6	5.932567
7	41°53′30″	7	7.100377
8	46°28′0″	8	8.331815
9	51°0′0″	9	9.775217

Table 5. Distortion Measurement Results of the HMD Optical System

		Relative Distortion (q)/%	
No.	View Field (ω)	Left View Field	Right View Field
0	0°0′0″	0.0	0.0
1	7°12′0″	0.0	0.0
2	13°28′0″	2.8	5.5
3	19°33′0″	3.6	6.7
4	25°31′30″	3.3	5.8
5	31°16′0″	1.0	4.0
6	36°51′0″	−1.1	1.1
7	41°53′30″	−3.2	−1.4
8	46°28′0″	−5.3	−4.0
9	51°0′0″	−8.6	−7.9

preprocessing circuitry mainly involves three steps: distortion preprocessing, translation correction, and distortion elimination. Its flow-process diagram is shown in Fig. 11.

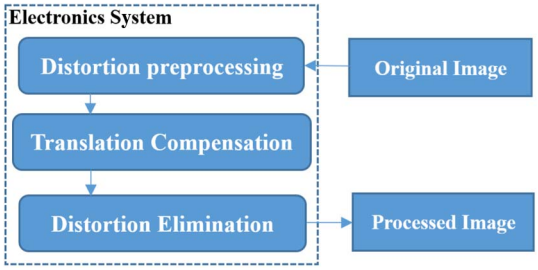

Fig. 11. Flow-process diagram of the electronics system.

A. Reverse Rotation and Translation Correction Model

The binocular structure in this study is composed of two monocular structures (left and right) in the form of a divergent partially overlapping FOV structure with a divergence angle of 18°. In such a structure, the different tilt directions between the left and right optical axes resulted in changes in the central FOV of the optical system. Such changes destroyed the FOV symmetry of the original system, such that people's eyes viewed the image information in different FOVs of the left and right

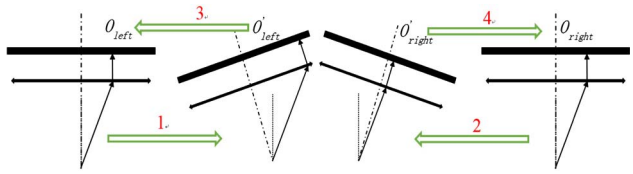

Fig. 12. Diagram of the binocular vision inconsistency.

optical systems, although what was observed was the same image information. In Fig. 12, processes 1 and 2 present the FOV deviation process during construction, and processes 1 and 2 present the calibration process using the model. The two thick solid lines in the figure indicate two simultaneously displayed LCDs. The two bidirectional arrow lines indicate the left and right HMD monocular optical systems. The two dashed–dotted lines represent the optical axes of the left and right optical systems, and the two dotted lines represent the binocular visual axes when human eyes are looking straight ahead. All the single arrow lines represent the light rays entering the eyes when looking sideways. When the two eyes are simultaneously observing images O_{left} and O_{right} on the right side, what the left eye sees through the left side is an image O'_{left} at the FOV edge of the left system; the right eye sees an image O'_{right} in the central FOV of the right system. In other words, the images seen by the two eyes differ greatly both in terms of content and quality at that time. Such a difference in binocular vision is called binocular vision inconsistency.

If binocular vision inconsistency is left uncorrected, it would affect people's binocular vision and impede the creation of a sense of immersion in the brain, thereby preventing the proposed device from achieving the VR simulation purpose. To solve this problem, a reverse rotation and translation calibration model was proposed, in which inconsistencies in binocular vision are corrected by the reverse rotation and translation of images on LCD pixels. The amount of reverse rotation translation $\Delta_{O'_{\text{left}} \to O_{\text{left}}}$ for correcting the image spot in the left side to the normal position was derived through the geometric relationship

$$\Delta_{O'_{\text{left}} \to O_{\text{left}}} = f \cdot \tan(\theta + \alpha) - f \cdot \tan(\theta). \quad (5)$$

The amount of reverse rotation translation $\Delta_{O'_{\text{right}} \to O_{\text{right}}}$ for correcting the image spot in the right side to the normal position was obtained as

$$\Delta_{O'_{\text{right}} \to O_{\text{right}}} = f \cdot \tan(\theta) - f \cdot \tan(\theta - \alpha), \quad (6)$$

where f is the focal length of the system, θ is the deflection angle of the visual axis, and α is the angular deflection of the optical axis ($\alpha = 18°$). Binocular vision inconsistencies can be corrected by adding the offset distance of the image obtained through Eqs. (2) and (3) to the algorithm and by adding reverse translation amounts $\Delta_{O'_{\text{left}} \to O_{\text{left}}}$ and $\Delta_{O'_{\text{right}} \to O_{\text{right}}}$ according to the computation results.

B. Geometric Distortion Correction

All trapezoidal distortions introduced in the distortion and reverse rotation model of the HMD optical system were image geometric distortions, which can be corrected with recognized methods. Common distortion correction methods include

two-step and planar methods, both of which consider the introduction of nonlinear parameters to optimize several parameters of linear solutions to improve the distortion elimination effect. Although accuracy is improved, the calibration process is complex, processing is slow, and timeliness is poor. After comprehensive consideration, the coordinate transformation method was utilized herein for distortion correction of 2D images. In the coordinate transformation method, the special relationship built based on image $g(u, v)$ or a set of base points is exploited to correct the distortion of another image $f(u', v')$. Coordinate transformation relation M was established by using several control points in the two images so that all the points in (u', v') coordinates can be corrected according to the geometric position of the standard image through M transform as

$$(u, v) = M \times (u', v'). \tag{7}$$

The specific process is shown in Fig. 13. Coordinate transformation matrix M was solved with the distortion measurement results. Then, original image A was input into the image processing program. The image processing procedure is essentially the inverse coordinate transform ($\mathbf{M^{-1}}$) operation of image A to obtain image C equivalent to having reverse distortion. Finally, users observe image C through the optical system, which is equivalent to completing the operation of coordinate transformation ($\mathbf{M}$), thereby eliminating the geometric distortions in the system and observing perfect images. Inset B presents the image observation effect by using the optical system solely.

Based on this principle, the system distortions were corrected twice. In the first correction, the residual distortions in the optical system were corrected. In the second correction, the trapezoidal distortions introduced were corrected after elimination of visual inconsistencies. The results of both corrections are satisfactory. Figures 14 and 15 demonstrate the contrast between the original picture (Fig. 14) and the electronically processed picture (Fig. 15).

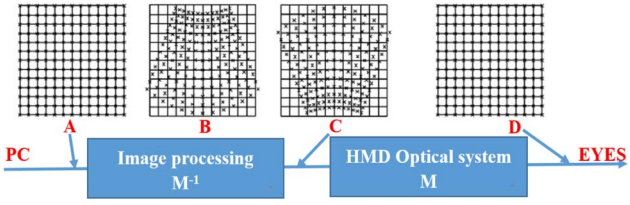

Fig. 13. Diagram of the distortion processing.

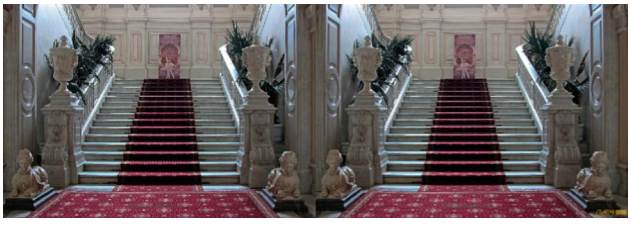

Fig. 14. Original picture; left and right eyes.

Fig. 15. Processed picture; left and right eyes.

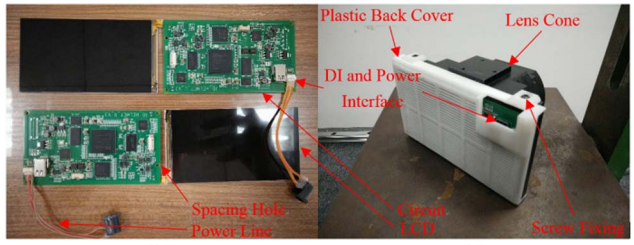

(a) (b)

Fig. 16. Electronic circuit board of high-speed digital image processing and optical tube with electronics. (a) Circuit board and LCD. (b) Tube with electronics.

Figure 16(a) presents the LCD and the electronic circuit board connected to it for high-speed digital image processing. Spacing holes were set at the four apical angles of the circuit board to fix the circuit board so that the circuit board could be fixed with a screw on the rear cover of the heat-resistant plastic obtained by 3D printing. Grooves are present in the optical tube so that the LCD screen could be securely mounted on the tube. The plastic rear cover and optical tube were also fixed with screws. After installation, the screws and nuts that fix the circuit board would press against the circuit board to position it at the optimal focal plane of the optical system. Figure 16(b) shows the monocular optical tube with electronics.

The high-speed digital image processing circuit board was connected to the control box via a data cable, and the control box was connected to the host via a VGA converter cable. During use, the host computer exerts control over the input images, and the control box exerts user control over the HMD LCD screen. Figures 17(a) and 17(b) present the control box, data cable, and corresponding data interfaces.

(a) (b)

Fig. 17. LCD control box and the HMD LCD display testing platform. (a) LCD control box; frontview. (b) LCD control box; rear view.

Fig. 18. HMD control interface on the computer; left and right eyes.

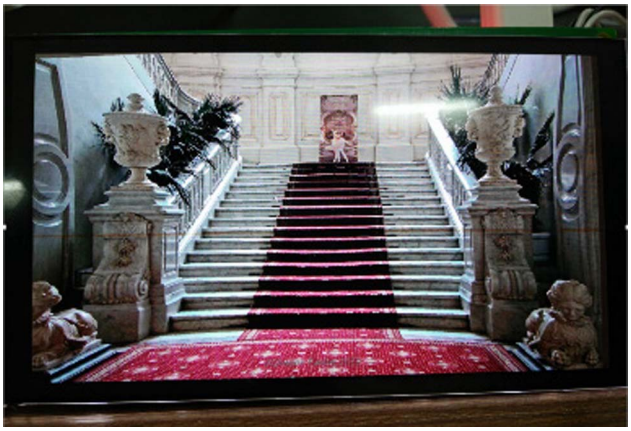

Fig. 19. Image display on the LCD; right eye.

Fig. 20. Picture of the material object.

The HMD electronic device can be initialized by connecting power in the order of the control box, host computer, and eyepiece circuit board. Figures 18 and 19 show the program interface on the host computer and the image displayed on the LCD by the right eye, respectively. The two images in the upper left corner of the interface are the original images input from the left and right eyes. What the interface shows on the whole is the electronically processed left and right eye images, i.e., images displayed on the LCD observed by the eyes of users through the optical system. The dialog box in the middle is for program control and monitoring purposes. Through this box, parameters such as image output mode, brightness, and contrast could be selected and controlled, and data such as image frame computation time could be monitored.

The high-performance VR HMD device developed in this study is shown in Fig. 20. Figure 21 shows the effect when the device is worn by the user.

Fig. 21. Impress drawing when a user is wearing the device.

5. CONCLUSION

A high-resolution (1920 × 1080), large-FOV [141.6°(H) × 73.08°(V)], not-fully-transparent VR HMD system for astronauts' space environment simulation training was successfully developed. Binocular high angular resolution and large field of view were achieved by employing aspheric technology to enhance the sense of immersion provided by the optical system. Continuously adjustable interpupillary distance was achieved within a 55 to 71 mm wide range through the use of a bidirectional rotatable thread structure to improve the universality and wearing comfort of the system. A correction model for image reverse rotations and translations was proposed. The model effectively addresses the binocular vision inconsistency in the divergent partially overlapping FOV HMD optical system. Meanwhile, the distortions in the optical system and the trapezoidal distortions introduced during image processing were measured and corrected. The present study offers a solution to reduced resolution to ensure a large field of view and a strong sense of immersion in not-fully-transparent VR HMD systems.

Funding. National Defense Basic Research Program (B1720132001).

Acknowledgment. The author is grateful to his team and tutor for the encouragement and help they provided during the process of this research. We are also grateful to The First Department of Space Optics, Changchun Institute of Optics, Fine Mechanics and Physics, Chinese Academy of Science; Shandong Institute of Aerospace Electronics Technology; and Key Laboratory of Human Factors Engineering, China Astronaut Training Center for the use of their equipment.

REFERENCES

1. X. P. Zhao, "Summarize of virtual reality," Chin. Sci. **39**, 2–26 (2009).
2. X. D. Li and B. Peng, "Developing summarize of virtual reality technology," Manage. Technol. Innovation **25**, 10–14 (2002).
3. O. Cakmakci and J. Rolland, "Head-worn displays: a review," J. Display Technol. **2**, 199–216 (2006).
4. P. Havig, J. Mcintire, and E. Geiselman, "Virtual reality in a cave: limitations and the need for HMDs," Proc. SPIE **8041**, 804107 (2011).

5. F. F. Zeng, *Technology of Virtual Reality* (Shanghai Jiao-tong University, 1997), pp. 34–36.
6. M. Li and F. Han, "Summarize of virtual reality technology," Software Guide **9**, 142–144 (2010).
7. D. W. Cheng, Y. T. Wang, H. Hua, and J. Sasian, "Design of a wide-angle, lightweight head-mounted display using free-form optics tiling," Opt. Lett. **36**, 2098–2100 (2011).
8. M. J. Chatten, J. B. Chatten, H. L. Task, D. G. Hopper, and B. A. Fath, "Development of a dichoptic foveal/peripheral head-mounted display with partial binocular overlap," Proc. SPIE **8041**, 80410F (2011).
9. J. M. Yang, W. Q. Liu, W. Z. Lv, F. He, Z. Wei, and Y. Kang, "Method of achieving a wide-field of view head-mounted display with small distortion," Opt. Lett. **38**, 2035–2037 (2013).
10. J. A. Piao, G. Li, M. L. Piao, and N. Kim, "Full color holographic optical element fabrication for waveguide-type head mounted display using photopolymer," J. Opt. Soc. Korea **17**, 242–248 (2013).
11. Q. Wang, D. Cheng, Y. Wang, H. Hua, and G. Jin, "Design, tolerance, and fabrication of an optical see-through head-mounted display with free-form surface elements," Appl. Opt. **52**, C88–C99 (2013).
12. B. Kress and T. Starner, "A review of head-mounted displays (HMD) technologies and applications for consumer electronics," Proc. SPIE **8720**, 87200A (2013).
13. H. Hua, X. D. Hu, and C. Y. Gao, "A high-resolution optical see-through head-mounted display with eye-tracking capability," Opt. Express **21**, 30993–30998 (2013).
14. H. Veron, P. J. Hezel, and D. A. Southard, "Head mounted displays for virtual reality," Proc. SPIE **2218**, 41–50 (1994).
15. K. Nemire, "Evaluating an immersive virtual environment prototyping and simulation system," Proc. SPIE **3012**, 408–416 (1997).
16. J. P. McIntire, G. L. Martinsen, P. L. Marasco, and P. R. Havig, "Virtual reality: a reality for future military pilotage," Proc. SPIE **7326**, 73260D (2009).
17. J. P. Rolland, "Wide-angle, off-axis, see-through head-mounted display," Opt. Eng. **39**, 1760–1767 (2000).
18. J. F. Morie, "When VR really hits the streets," Proc. SPIE **9012**, 90120B (2010).
19. C. Gao, Y. Lin, and H. Hua, "Optical see-through head-mounted display with occlusion capability," Proc. SPIE **8735**, 87350F (2013).
20. K. P. Thompson and J. P. Rolland, "A page from the drawer: how Roland shack opened the door to the aberration theory of freeform optics," Proc. SPIE **9186**, 91860A (2014).
21. D. Hayes, C. Turczynski, and J. Rice, "Virtual-reality-based educational laboratories in fiber optic engineering," Proc. SPIE **9289**, 928921 (2014).